Wing-Flutter Calculations with the CAP-TSD Unsteady Transonic Small-Disturbance Program

Robert M. Bennett,* John T. Batina,† and Herbert J. Cunningham‡
NASA Langley Research Center, Hampton, Virginia

The paper describes the application and assessment of the recently developed CAP-TSD transonic small-disturbance code for flutter prediction. The CAP-TSD program has been developed for aeroelastic analysis of complete aircraft configurations and was previously applied to the calculation of steady and unsteady pressures with favorable results. Flutter calculations are presented for two thin, swept-and-tapered wing planforms with well-defined modal properties. The calculations are for Mach numbers from low subsonic to low supersonic values, including the transonic range, and are compared with subsonic linear theory and experimental flutter data. The CAP-TSD flutter results are generally in good agreement with the experimental values and are in good agreement with subsonic linear theory when wing thickness is neglected.

Nomenclature

b_0 = reference length, $c_r/2$
c_r = reference length; root chord
ΔC_p = coefficient of lifting pressure, $\Delta p/(\rho U^2/2)$
f = frequency, Hz
k = reduced frequency, $\omega b_0/U$
M = freestream Mach number
Δp = lifting pressure; positive up
$q_i(t)$ = generalized coordinate of motion for mode i
t = time
U = freestream speed
x,y,z = right-hand orthogonal coordinates
μ = ratio of wing mass to mass of air in the truncated cone that encloses the wing
ρ = freestream flow density
ϕ = disturbance velocity potential
$\omega,\omega_i,\omega_\alpha$ = circular frequency, in general; of mode i and of the first torsion mode, respectively, rad/s

Introduction

SIGNIFICANT research effort is currently underway to develop computational fluid dynamics (CFD) methods for refined unsteady aerodynamics for aeroelastic analysis. Edwards and Thomas[1] have given a recent survey, for example, on computational methods for unsteady transonic flows with emphasis on applications to aeroelastic analysis and flutter prediction. The transonic speed range is of primary interest because the flutter dynamic pressure is typically critical (i.e., lower) there. The main effort, especially for three-dimensional configurations, has been at the transonic small-disturbance (TSD) equation level, of which the XTRAN3S program is an important example.[2] For the higher equation levels such as the Euler and Navier–Stokes, efforts on aeroelastic applications have been limited to simple two-dimensional airfoils because of the larger computational cost involved. Two recent efforts are reported by Bendiksen and Kousen[3] and by Wu et al.[4]

The TSD formulation has the advantage of relatively low cost and the simplicity of the gridding and geometry preprocessing while retaining much of the essential features of the physics of unsteady transonic flow. Batina[5] has described the development of a time-accurate approximate factorization (AF) algorithm applied to the TSD equation that is very stable and is efficient on current supercomputers with vector arithmetic. The AF algorithm has subsequently been developed into a new computer program called CAP-TSD (Computational Aeroelasticity Program-Transonic Small Disturbance) for transonic aeroelastic analysis of complete aircraft configurations.[6] CAP-TSD has been used to calculate steady and unsteady pressures on wings and configurations at subsonic, transonic, and supersonic Mach numbers. Comparisons of these results with other methods and with experimental data have been favorable.[6,7] However, the CAP-TSD code has been developed primarily for aeroelastic analysis. Such analysis involves the coupling of the aerodynamics with the structural characteristics of the configuration under consideration. The resulting equations of motion for a time-domain or time-marching aeroelastic analysis are based upon the aircraft natural vibration modes. These equations are integrated in time along with the finite-difference solution of the flowfield. Initial conditions for each mode are input and free decay transients are calculated. Aeroelastic stability is then deduced from the free decay records or time histories. Both the underlying theory and the numerical procedures require evaluation. The purpose of the present paper is to report on the results of an evaluation of the application of CAP-TSD for flutter calculations for some simple cantilevered wings as a necessary first step in flutter validation before treatment of more complex configurations.

Two wing planforms are treated for flutter comparisons. One planform is a series of 45-deg swept wings,[8] which are an AGARD standard configuration for aeroelastic analysis.[9] The other planform is a clipped delta wing[10,11] that was used in some early active controls work. The physical properties and experimental flutter boundaries for these wings are well defined, which is essential for validation purposes. In addition to comparisons with experimental data, results from CAP-TSD with wing thickness neglected are compared with subsonic linear theory which should give corresponding results. In an earlier paper,[12] generalized aerodynamic forces for one of the

Presented as Paper 88-2347 at the AIAA/ASME/ASCE/AHS/ASC 29th Structures, Structural Dynamics, and Materials Conference, Williamsburg, VA, April 18–20, 1988; received April 7, 1988; revision received Dec. 8, 1988;

*Senior Research Engineer, Unsteady Aerodynamics Branch, Structural Dynamics Division. Associate Fellow AIAA.
†Research Scientist, Unsteady Aerodynamics Branch, Structural Dynamics Division. Senior Member AIAA.
‡Research Engineer, Unsteady Aerodynamics Branch, Structural Dynamics Division. Member AIAA.

45-deg wings computed from CAP-TSD were shown to be in good agreement with linear theory forces over a broad range of reduced frequency. There was also good agreement of the flutter boundary calculated with CAP-TSD with the boundaries obtained from linear theory and from experiment. These flutter results[12] and additional calculations are included herein in order to present a complete set of calculations for the series of 45-deg wings.

In this paper, a brief description of CAP-TSD and the aeroelastic analysis and an overall description of the wings analyzed are given; the flutter results are described.

Computational Procedures

In this section, the computational procedures are described including the CAP-TSD program, the aeroelastic equations of motion, the time-marching solution of these equations, and the modal identification of the resulting free-decay transients.

CAP-TSD Program

The CAP-TSD program is a finite-difference program that solves the general-frequency modified TSD equation. The TSD potential equation is defined by

$$M^2(\phi_t + 2\phi_x)_t = [(1-M^2)\phi_x + F\phi_x^2 + G\phi_y^2]_x + (\phi_y + H\phi_x\phi_y)_y + (\phi_z)_z \tag{1}$$

Several choices are available for the coeffficients F, G, and H depending upon the assumptions used in deriving the TSD equation. For transonic applications, the coefficients are herein defined as

$$F = -\tfrac{1}{2}(\gamma+1)M^2, \qquad G = \tfrac{1}{2}(\gamma-3)M^2$$
$$H = -(\gamma-1)M^2 \tag{2}$$

The linear potential equation is recovered by simply setting F, G, and H equal to zero.

Equation (1) is solved within CAP-TSD by an AF algorithm developed by Batina.[5] In Refs. 5–7, the AF algorithm was shown to be efficient for application to steady or unsteady transonic flow problems. It can provide accurate solutions in only several hundred time steps yielding a significant computational cost savings when compared to alternative methods. Recently, several algorithm modifications have been made that improve the stability of the AF algorithm and the accuracy of the results.[13,14] These algorithm modifications include 1) Engquist-Osher (E-O) type-dependent differencing to more accurately and efficiently treat regions of supersonic flow, 2) extension of the E-O switch for second-order-accurate upwind differencing in supersonic regions to improve the accuracy of the results, 3) nonreflecting far-field boundary conditions for more accurate unsteady applications, 4) several modifications which accelerate convergence to steady state, and 5) entropy and vorticity modifications for treating strong shock waves more accurately. The capabilities employed in the present study include the E-O switch and the nonreflecting boundary conditions. The CAP-TSD program can treat configurations with combinations of lifting surfaces and bodies including canard, wing, tail, control surfaces, tip launchers, pylons, fuselage, stores, and nacelles. Steady and unsteady pressures have been presented for several complex aircraft configurations in Ref. 6. The calculated results were in good agreement with available experimental pressure data which validated CAP-TSD for multiple component applications with mutual aerodynamic interference effects.

Equations of Motion

The aeroelastic equations of motion that have been incorporated in CAP-TSD are based on a right-hand orthogonal coordinate system with the x-direction defined as positive downstream and the z-direction positive upward. The presentation herein is limited to the case of an isolated wing with motion in the z-direction from an undisturbed position in the $z=0$ plane. The equations of motion may be written as

$$M\ddot{q} + C\dot{q} + Kq = Q \tag{3}$$

where q is a vector of generalized displacements, M is the generalized mass matrix, C is the damping matrix, and K is the stiffness matrix. Q is the vector of generalized forces defined by

$$Q_i = \frac{\rho U^2}{2} c_r^2 \int_s \frac{\Delta p h_i \, dS}{\rho U^2/2c_r^2}$$

where Δp is the lifting pressure and h_i is the vibration mode shape. Equation (3) is rewritten as

$$\ddot{q} = -M^{-1}Kq - M^{-1}C\dot{q} + M^{-1}Q \tag{4}$$

Time-Marching Aeroelastic Solution

The aeroelastic solution procedure implemented within CAP-TSD for integrating Eq. (4) is similar to that described by Edwards et al.[15] Reference 15 describes an aeroelastic solution for a two-dimensional, two-degree-of-freedom system in terms of a state equation formulation. Here, by a parallel formulation, a linear state equation is developed from Eq. (4). Each element of Eq. (4) is a normal mode equation that may be expressed in first-order state-space form as

$$\dot{x}_i = Ax_i + Bu_i \tag{5}$$

where

$$x_i = [q_i \dot{q}_i]^T$$

$$A = \begin{bmatrix} 0 & 1 \\ -m_i^{-1}k_i & -m_i^{-1}c_i \end{bmatrix}$$

$$B = m_i^{-1}\frac{\rho U^2}{2} c_r^2 \begin{bmatrix} 0 \\ 1 \end{bmatrix}$$

$$u_i = \left[\int_s \Delta C_p h_i \, dS/c_r^2\right]$$

$$\Delta C_p = \frac{\Delta p}{\rho U^2/2}$$

In these definitions, m_i, c_i, and k_i are elements of the mass, damping, and stiffness matrices, respectively, corresponding to mode i. Equation (5) is a finite-dimensional linear differential equation and its solution is given by

$$x_i(t) = \Phi(t)x_i(0) + \int_o^t \exp[A(t-\tau)]Bu(\tau)d\tau \tag{6}$$

The state-transition matrix $\Phi(t) = \exp[At]$, in general, can be calculated to any assigned accuracy by using a sufficient number of terms of the series expansion of the matrix exponential function. For the aeroelastic problem considered here, $\Phi(t)$ is computed exactly using simple closed-form expressions for each element of the matrix. As explained in Ref. 15, the first term in Eq. (6) is the homogeneous response portion of Eq. (5), while the second term is a convolution integral that represents the forced response. Numerically, the solution is advanced from any time step n to step $n+1$, by

$$x_i[(n+1)\Delta t] = \Phi(\Delta t)x_i(n\Delta t) + \int_{n\Delta t}^{(n+1)\Delta t} \exp\{A[(n+1)\Delta t - \tau]\}Bu(\tau)\,d\tau \tag{7}$$

where Δt is the time step. The simplest approximation for the integral is to assume that $u(\tau)$ is constant, $u(\tau) = u(n\Delta t)$. A

better approximation is to assume that u varies linearly from u^n to u^{n+1}, estimating u^{n+1} as $u^n+(u^n-u^{n-1})$. The resulting algorithm is

$$x_i^{n+1} = \Phi x_i^n + \theta B(3u^n - u^{n-1})/2 \quad (8)$$

where θ is the integral of the state-transition matrix Φ. Reference 16 describes a comparative evaluation of seven alternative structural integration algorithms including that of Eq. (8). The modified state-transition matrix integrator of Eq. (8) was shown to be superior to the others in terms of numerical stability and accuracy.

For aeroelastic analysis, two steps are generally required in performing the calculations. In the first step, the steady-state flowfield is calculated to account for wing thickness, camber, and mean angle of attack, thus providing the starting flowfield for the aeroelastic analysis. The second step is to prescribe an initial disturbance to begin the structural integration. Experience has shown that using disturbance velocities in one or more modes, rather than displacements, is distinctly superior in avoiding nonphysical, strictly numerical transients and their possible associated instabilities. For the applications presented herein, 750–1000 time steps were typically used to compute about 3–6 cycles of the dominant flutter mode. In determining a flutter point, the freestream Mach number M and the associated freestream speed U were held fixed. A judiciously chosen value of the dynamic pressure $\rho U^2/2$ is used and free decay transients are computed. These resulting transients of the generalized coordinates are analyzed for their content of damped or growing sine waves, with the rates of growth or decay indicating whether the dynamic pressure is above or below the flutter value. This analysis then indicates whether to increase or decrease the value of dynamic pressure in subsequent runs to determine a neutrally stable result. Further details are given in the following section on modal identification. Typically, the finite-difference solution used is of the order of 200,000 grid points. Each transient generated required about 15 min of central processing time on the CDC VPS 32 computer.

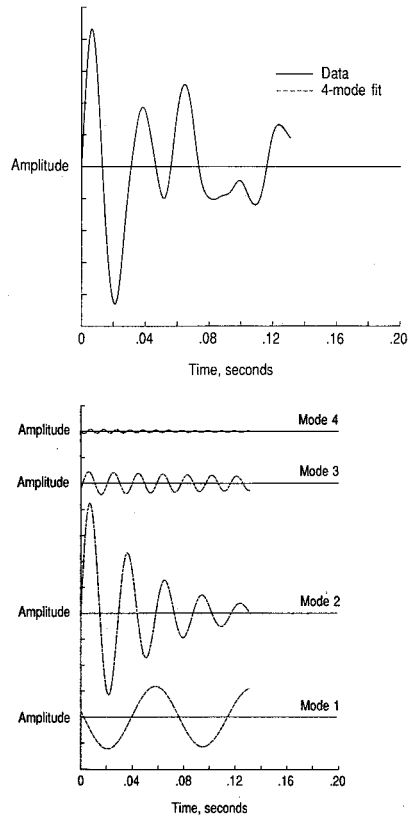

Fig. 1 Sample modal identification from free decay transient for the 45-deg swept wing calculated using CAP-TSD: a) aeroelastic transient and least squares curve fit; and b) component modes from curve fit.

Modal Identification

As previously mentioned, CAP-TSD generates free decay transients that must be analyzed for the modal stability characteristics. An example transient for a 45-deg sweptback wing, calculated using CAP-TSD, is shown in Fig. 1a. All four modes used in the analysis were excited by specifying an initial condition for each modal velocity, which produces a complicated decay record. This record is analyzed using a least-squares curve-fit of the response data with complex exponential functions. The program utilized is a derivative of the one described in Ref. 17. The components of the transient of Fig. 1a are plotted in Fig. 1b to the same scale. The free decay properties of each mode for this condition are readily apparent. A sufficient range of dynamic pressure must be considered to determine all relevant flutter points. In cases that involve a large number of modes, it has been found that the modal identification is simplified if only the principle flutter mode is excited.

Wing-Flutter Test Cases

The two wing planforms used for flutter comparisons are briefly described including the airfoil shape and vibration modes.

45-deg Swept Wings

The wings being analyzed are semispan wind-tunnel-wall-mounted models[8] that have a quarter-chord sweep angle of 45 deg (leading edge sweep of 46.3 deg), a panel aspect ratio of 1.65, and a taper ratio of 0.66. This series of wings was tested in the Transonic Dynamics Tunnel (TDT) at NASA Langley Research Center and is an AGARD standard aeroelastic configuration.[9] A planview of the wing is shown in Fig. 2 and a photograph of a model mounted in the TDT is shown in Fig. 3. The wings have a NACA 65A004 airfoil section and were constructed of laminated mahogany. In order to obtain flutter for a wide range of Mach number and density conditions in the TDT, some of the wings had holes drilled through the wing to reduce the stiffness. To maintain the airfoil shape, the holes were filled with a rigid foam plastic as can be seen in Fig. 2. The weakened wings are denoted WEAK1, etc., with the numerical suffix used to distinguish the different models. Models without the holes are called SOLID1, etc., with the numerical suffix also indicating a different model. The models in each series were designed and fabricated to be as identical to one another as possible. Both series of models were tested in air and Freon® test media.

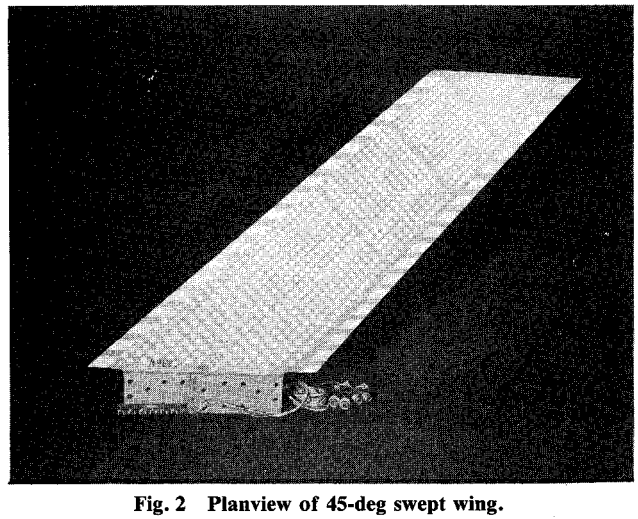

Fig. 2 Planview of 45-deg swept wing.

®Freon: Registered trademark of E. E. duPont de Nemour and Co., Inc.

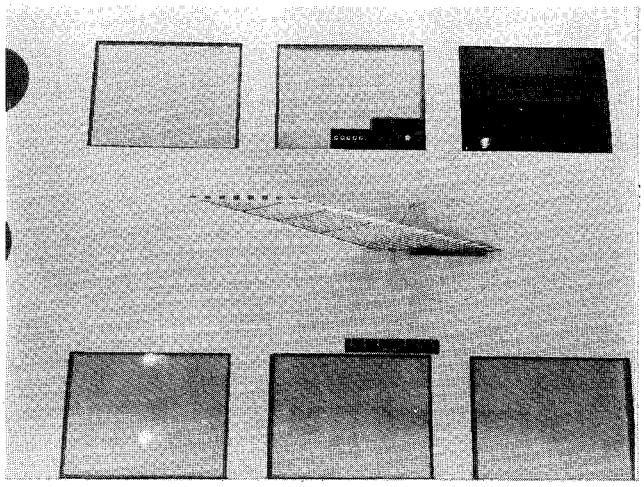

Fig. 3 A 45-deg swept wing in the NASA Langley Transonic Dynamics Tunnel.

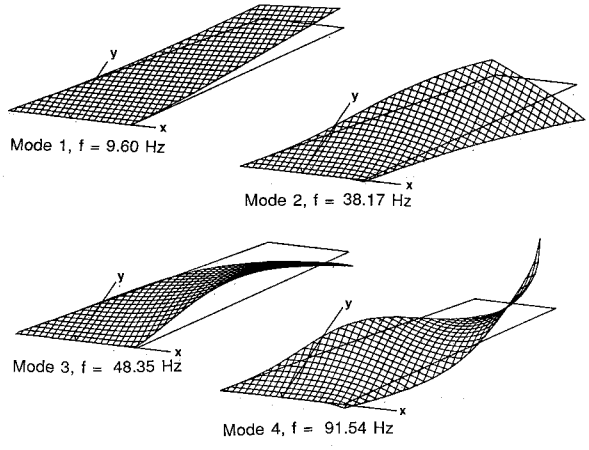

Fig. 4 Oblique projections of natural vibration modes of 45-deg swept wing WEAK3.

Mode shapes for both WEAK3 and SOLID2 models were calculated with a finite-element analysis and are given in Ref. 9. Figure 4 shows oblique projections for the four natural modes used to model wing WEAK3 structurally. These modes, numbered 1–4, represent first bending, first torsion, second bending, and second torsion, respectively. The modal frequencies range from 9.60 Hz for the first bending mode to 91.54 Hz for the second torsion mode.

The corresponding oblique projections of the modes for wing SOLID2 are shown in Fig. 5. The modes for this wing are generally similar to the modes for WEAK3 but differ in detail. The first four frequencies range from 14.12–122.26 Hz. The higher frequencies in the SOLID wings reflect the increased stiffness level over the WEAK series of wings.

Clipped Delta Wing

The second wing analyzed is a clipped delta wing model that was also tested in Freon in the NASA Langley TDT.[10,11] A view of the model mounted in the TDT is presented in Fig. 6. The wing has a leading-edge sweep angle of 50.5 deg, a panel aspect ratio of 1.24, and a taper ratio of 0.142. The airfoil section is a circular arc with a maximum thickness-to-chord ratio of 0.03. The wing was constructed of a load-carrying plate structure with cutouts to simulate a beam structure and was covered with balsa wood which was contoured to the required airfoil shape. The model also had two slender underwing bodies to simulate engine nacelles. The total mass of these bodies was about the same as the total mass of the wing. A fuselage fairing was used to ensure that the wing root was outside the tunnel-wall boundary layer (Fig. 6).

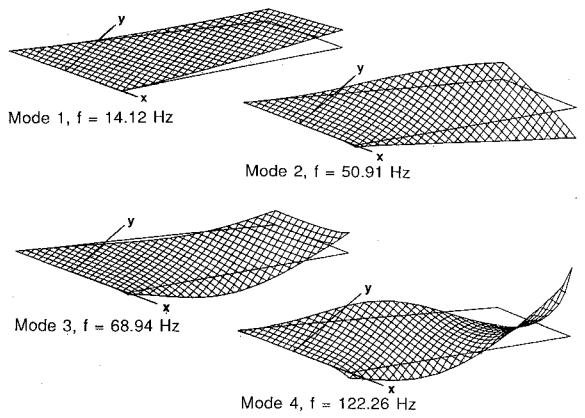

Fig. 5 Oblique projections of natural vibration modes of 45-deg swept wing SOLID2.

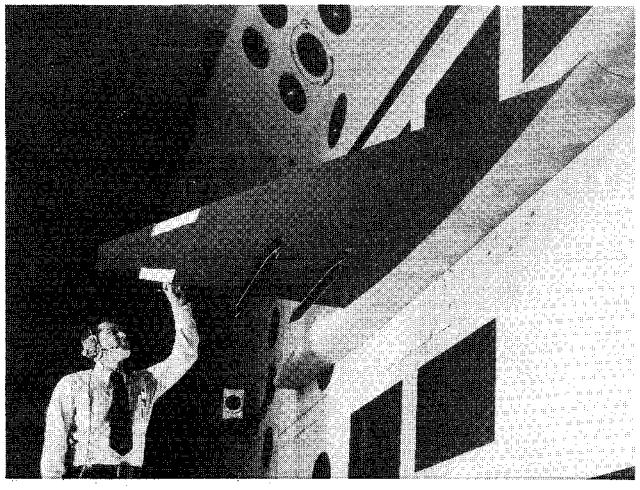

Fig. 6 Clipped delta wing model in the NASA Langley Transonic Dynamics Tunnel.

Nine natural vibration modes and their associated generalized masses were measured.[11] Oblique projections of these modes are shown in Fig. 7. These modes have natural frequencies that range from 7.8 Hz for mode 1 to 58.1 Hz for mode 9. The nacelle masses have a large effect on the mode shapes particularly in the inboard region of the wing. It also should be noted that mode 6 contains a large torsion component near the tip.

Results and Discussion

The flutter results are presented for the series of 45-deg wings first, followed by the results for the clipped delta wing. In each case, three sets of analytical results are presented and compared to the experimental flutter characteristics. The analytical results correspond to 1) CAP-TSD results obtained using the linear potential equation [$F = G = H = 0$ in Eq. (1)] and modeling the wing as a flat plate, 2) CAP-TSD results obtained using the complete nonlinear (TSD) equation and including wing thickness, and 3) subsonic-kernel-function results from program FAST[18] using 100 collocation points (10 in chordwise and spanwise directions) and the maximum quadrature option. The results from 1 and 3 should, of course, agree as the same equations are being solved by FAST and by CAP-TSD with the linear equation option.

Flutter Results for the 45-Deg Swept Wings

Both WEAK and SOLID wings were tested in air and Freon.[8] Calculations using CAP-TSD were made for each wing in air or Freon as appropriate. The measured flutter

boundaries for the WEAK series of wings is more extensive and will be discussed first.

WEAK Wings in Air

Comparisons of flutter characteristics from the linear calculations with the experimental data are given in Fig. 8. Plots of flutter-speed index [defined as $U/(b_o\omega_\alpha\sqrt{\mu})$] and nondimensional flutter frequency (defined as ω/ω_α) as functions of freestream Mach number are shown in Figs. 8a and 8b, respectively. The experimental data are all for wing WEAK3 except for the point at $M=0.338$, which is for wing WEAK4. The experimental flutter data defines a typical transonic flutter "dip" with the bottom near $M=1.0$ for this case. (Note that these results are shown with an expanded scale.) The bottom of the dip in flutter-speed index (Fig. 8a) was defined by the approach to the M = 1.072 flutter point during the wind-tunnel operation. Results from the CAP-TSD (linear) code are presented at 12 values of M covering the entire Mach number range over which the flutter data was measured. Results from the FAST program are presented for the limited range $0.338 \le M \le 0.96$ since the method is restricted to subsonic freestreams. Overall, the linear CAP-TSD results compare well with the experimental data for subsonic as well as supersonic Mach numbers. Note that the subsonic FAST results are also in good agreement with the data. Such a result is not unexpected for this very thin wing of moderate sweep and taper at zero angle of attack. It does indicate that the wing properties are well defined for benchmark purposes.

In the subsonic Mach number range, the CAP-TSD and FAST calculations predict a slightly unconservative flutter speed, except at $M=0.338$, by as much as 2% (Fig. 8a), and a higher flutter frequency (Fig. 8b) in comparison with the experimental data. In general though, the linear CAP-TSD results agree well with the FAST results in both flutter speed and frequency. The good agreement in this three-way correlation betwen experiment, linear theory, and CFD flutter results gives confidence in the CAP-TSD code for flutter prediction. For this test in air, the mass ratio varies from about 12 at low Mach numbers to about 250 in the transonic range. The corresponding k values range from about 0.3 at the low Mach numbers to about 0.08 in the transonic range. Thus, the flutter in the transonic range for this wing is at a relatively low k value.

Comparisons of flutter characteristics from the linear and nonlinear CAP-TSD calculations with the experimental data are given in Fig. 9. Figure 9a shows flutter-speed index vs Mach number, and Fig. 9b shows nondimensional flutter frequency vs Mach number. Three flutter points are plotted from the nonlinear CAP-TSD calculations corresponding to $M=0.678$, 0.901, and 0.96. Comparisons between the two sets of CAP-TSD results show differences due to wing thickness and nonlinear effects. With increasing Mach number, these differences become larger. For example, at $M=0.678$, 0.901, and 0.96, the flutter-speed index decreased by 1, 5, and 19%, respectively, as shown in Fig. 9a. Similar decreases also occur in the flutter frequency (Fig. 9b). The decrease in flutter speed at $M=0.901$ is largely due to including wing thickness since there are no supersonic points in the flow calculations at this condition. The decrease in flutter speed at $M=0.96$ is attributed to both wing thickness and nonlinear effects since an

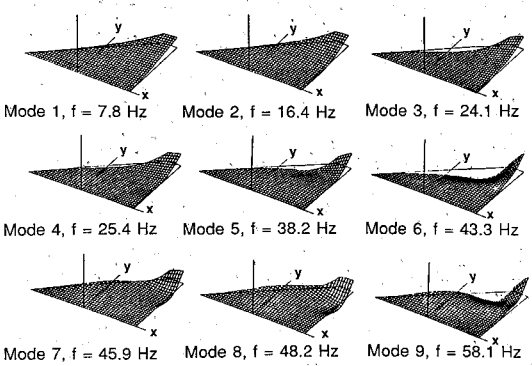

Fig. 7 Oblique projections of natural vibration modes of clipped delta wing model.

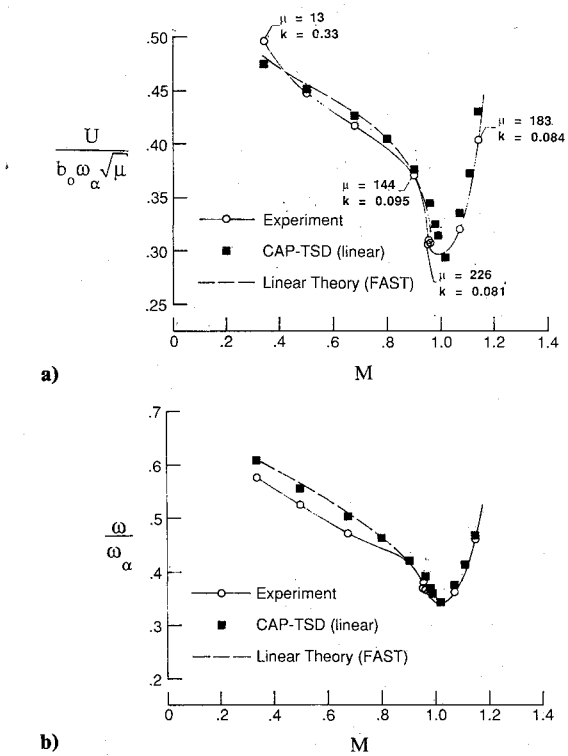

Fig. 8 Comparisons between linear flutter calculations with experimental data for the 45-deg swept WEAK wings in air: a) flutter-speed index vs Mach number; and b) flutter-frequency ratio vs Mach number.

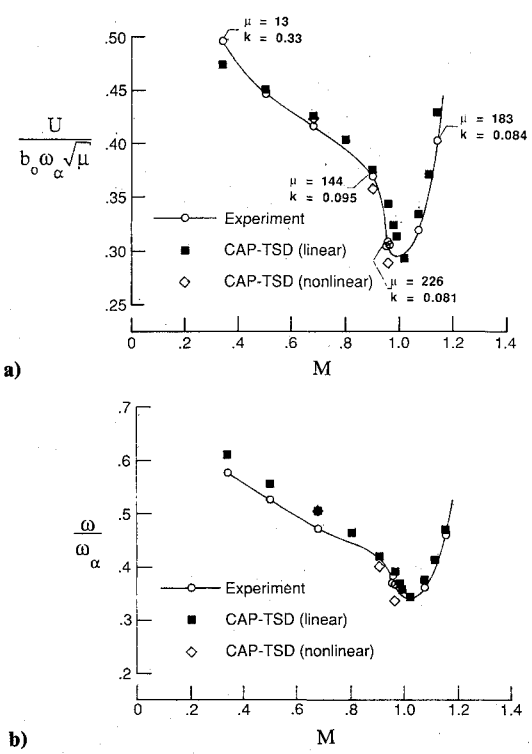

Fig. 9 Comparisons between linear and nonlinear CAP-TSD flutter predictions with experimental data for the 45-deg swept WEAK wings in air: a) flutter-speed index vs Mach number; and b) flutter-frequency ratio vs Mach number.

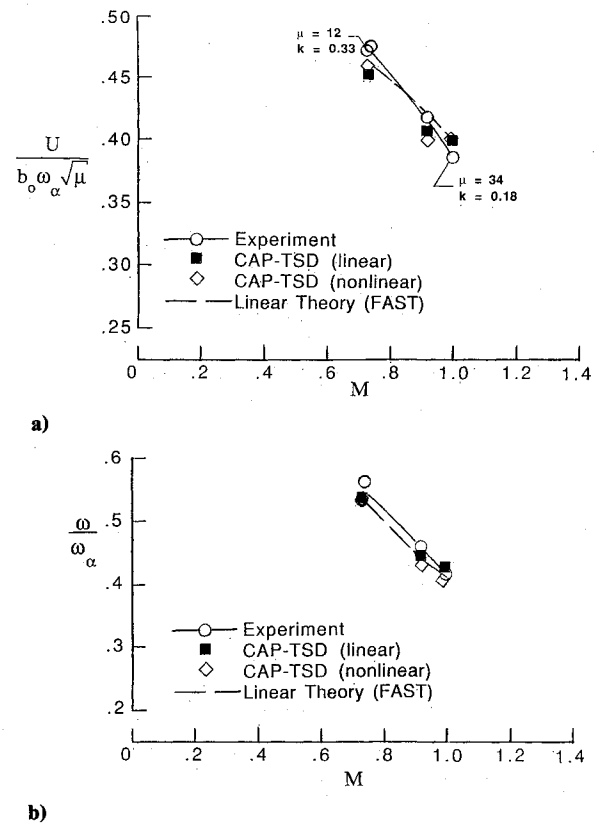

Fig. 10 Comparisons between flutter calculations and experimental data for the 45-deg swept WEAK wings in Freon: a) flutter-speed index vs Mach number; and b) flutter-frequency ratio vs Mach number.

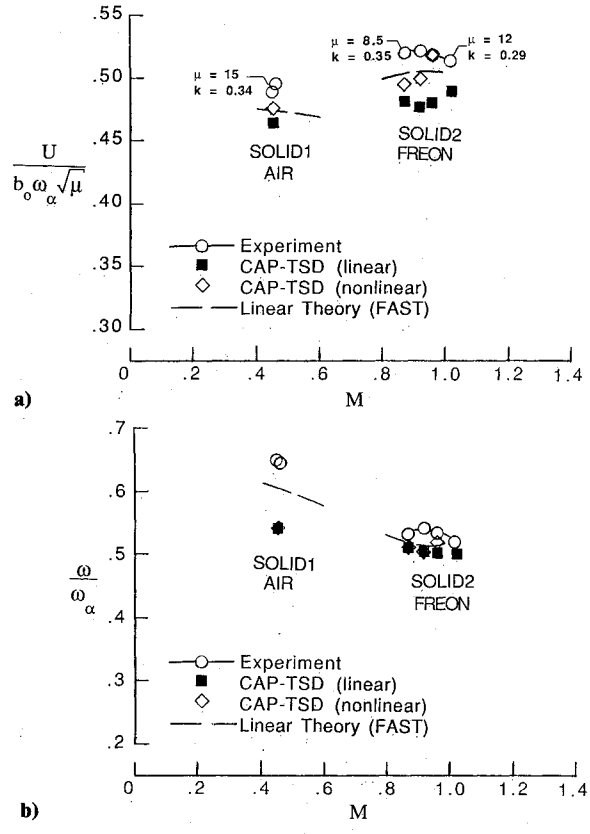

Fig. 11 Comparisons between flutter calculations and experimental data for the 45-deg swept SOLID wings: a) flutter-speed index vs Mach number; and b) flutter-frequency ratio vs Mach number.

embedded supersonic region of moderate size was calculated in the wing tip region. The nonlinear CAP-TSD results at both $M = 0.901$ and 0.96 are slightly conservative in comparison with the experimental flutter-speed index value. Nonetheless, the nonlinear CAP-TSD flutter results compare favorably with the experimental data, which is the first step toward validating the code for general transonic aeroelastic applications.

WEAK Wings in Freon

The flutter characteristics for wings WEAK5 and WEAK6 are presented in Figs. 10a and 10b. Experimental flutter points are shown for Mach numbers near 0.74, 0.92, and 1.00. These wings in Freon do not show the strong dip in flutter speed near $M = 0.90$ exhibited by the wings in air, but do indicate a significant decrease in flutter speed in the transonic range. Results from the subsonic kernel function and CAP-TSD with and without thickness are shown (Figs. 10a and 10b). Each of the three results are in good overall agreement with the experimental flutter speeds and frequencies. The effect of thickness in the CAP-TSD results is less than 2% in flutter-speed index and thus relatively small at all three Mach numbers. The mass ratios for these wings tested in the more dense Freon vary from about 12–34 as Mach number increases from 0.73–1.0. The corresponding reduced frequencies vary from 0.34–0.18. Less effect of thickness normally would be expected at these higher k values than for the tests in air with lower reduced frequencies.

SOLID Wings

The experimental flutter characteristics for wings SOLID1 and SOLID2 are compared with the corresponding analytical results in Figs. 11a and 11b. Wing SOLID1 was tested in air and two data points near $M = 0.45$ are shown. Wing SOLID2 was tested in Freon and four data points for Mach numbers from 0.87–1.02 are shown.

The results from FAST for SOLID1 are shown for constant mass ratio (14.6) on the left part of Figs. 11a and 11b. Note again that these results are shown with an expanded scale. The flutter speed calculated by FAST is 3% lower than the data and the frequency about 6% lower. The corresponding results from CAP-TSD are somewhat lower and show a modest effect of thickness. Overall, the agreement is somewhat less satisfactory than that for the other wings but still fairly good. The flutter reduced frequency for this wing is about 0.30.

The corresponding results for SOLID2 are shown in the right portion of Figs. 11a and 11b. The results from FAST are in good agreement with the high subsonic data and are about 3% lower in flutter-speed index than experiment. The corresponding CAP-TSD linear calculations are about 4% lower in flutter-speed index than the FAST results but with good agreement in flutter-frequency ratio. The effect of thickness shown by the CAP-TSD nonlinear calculations is stabilizing by about 3% at $M = 0.87$ to 8% at $M = 0.96$. A stabilizing effect of thickness at transonic Mach numbers is surprising. The mass ratio for this wing ranges from 8.5–12 and the flutter reduced frequency ranges from about 0.35–0.29 as Mach number increases from 0.87–1.02. The flutter trends for this wing are quite different than those for WEAK3 in air and in Freon. This result may possibly be a consequence of the lower mass ratio and the higher reduced frequencies for this model. For example, for the WEAK3 model in air at high mass ratio and low reduced frequency, there is a large transonic dip and a strong destabilizing effect of thickness. In Freon, with a decrease in mass ratio and higher reduced frequency, the transonic dip is reduced and there is only a small effect of thickness. For SOLID2 in Freon, where the mass ratio is further decreased and reduced frequency is even larger, there appears to be a stabilizing effect of thickness. Thus, the transonic effects for this wing appear to depend strongly on mass ratio and the resulting reduced frequency of flutter.

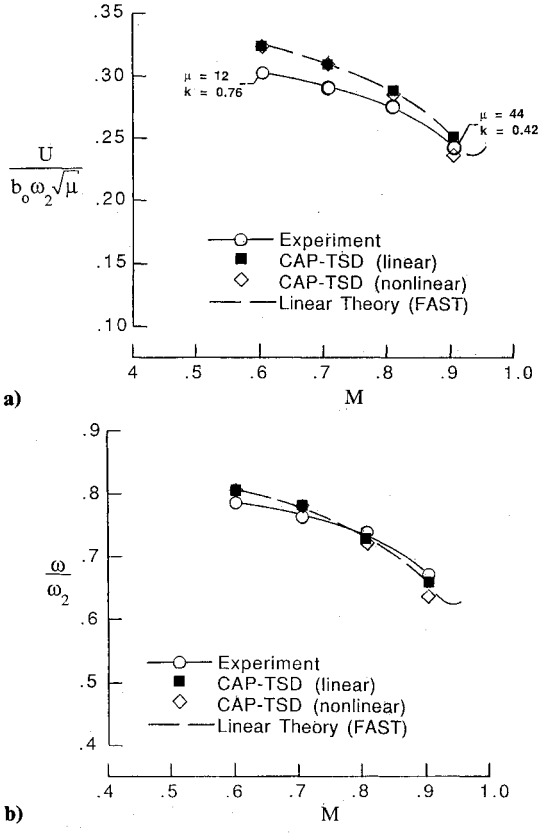

Fig. 12 Comparisons between flutter calculations and experimental data for the clipped delta wing: a) flutter-speed index vs Mach number; and b) flutter-frequency ratio vs Mach number.

Flutter Results for the Clipped Delta Wing

The clipped delta wing analyzed is that denoted as Wing C of Ref. 11. This planform represents an increase in complexity from the 45-deg swept wings from the standpoint of the increased sweep and taper of the planform and the number and complexity of the vibration modes. Previous calculations[11] for this model have shown that six modes are required for flutter analysis and all nine were included in the present calculations. The same sequence of calculations has been performed for the clipped delta wing as was performed for 45-deg swept wings.

There were four measured flutter points for this wing as shown in Figs. 12a and 12b. These flutter points are near $M = 0.6$, 0.7, 0.8, and 0.9 and do not determine the bottom of the transonic dip in flutter speed. Tests on some similar wings[11] indicated the bottom of the dip to be near $M = 0.92$. The experimental values of mass ratio range from 12 at $M = 0.60$ to 44 at $M = 0.91$ with the corresponding reduced frequencies (based on root semichord) ranging from 0.76–0.42. The flutter speeds from FAST are higher than the experimental flutter-speed index ranging from 4% at $M = 0.907$ to 7% at $M = 0.603$ as shown in Fig. 12a. The flutter-frequency ratios are in good agreement with experiment (Fig. 12b). The FAST results also show a dip near $M = 0.94$ that is sensitive to mass ratio. The corresponding results from CAP-TSD using the linear equation and flat plate wing for the experimental Mach numbers are essentially identical to the results from FAST, which further verifies the CAP-TSD program. Inclusion of thickness in the CAP-TSD analysis results in essentially no effect at $M = 0.603$ to a 6% reduction in flutter speed at $M = 0.907$, which improves the agreement with the experimental flutter speed.

Concluding Remarks

In an effort to assess the accuracy of the CAP-TSD program for aeroelastic applications, flutter calculations have been made for several wings of two different planforms varying in sweep and taper and with thin airfoil sections. One planform is a series of 45-deg swept wings, which is an AGARD standard configuration for aeroelastic analysis. The other planform is a clipped delta wing that was used in some early active controls work. The physical properties and experimental flutter boundaries for these wings are well defined for validation purposes.

Extensive comparisons were made between the results of CAP-TSD using the linear equation and no airfoil thickness and the results obtained from a subsonic kernel function analysis. The comparisons indicated good to excellent agreement for these analyses. The effect of thickness for these thin wings as determined from CAP-TSD was relatively small and improved the agreement with experiment.

The calculations with CAP-TSD covered an extensive Mach number range from low subsonic to low supersonic values with good overall agreement with experiment. Both wings have very thin airfoil sections and consequently the effects of thickness were modest. Further analysis for thick and supercritical wings is needed.

References

[1]Edwards, J. W. and Thomas, J. L., "Computational Methods for Unsteady Transonic Flows," AIAA Paper 87-0157, Jan. 1987.

[2]Borland, C. J. and Rizzetta, D. P., "Nonlinear Transonic Flutter Analysis," *AIAA Journal,* Vol. 20, Nov. 1982, pp. 1606–1615.

[3]Bendiksen, O. O. and Kousen, K., "Transonic Flutter Analysis Using the Euler Equations," AIAA Paper 87-0911, April 1987.

[4]Wu, J. C., Kaza, K. R. V., and Sankar, N. L., "A Technique for the Prediction of Airfoil Flutter Characteristics in Separated Flows," AIAA Paper 87-0910, April 1987.

[5]Batina, J. T., "An Efficient Algorithm for Solution of the Unsteady Transonic Small-Disturbance Equation," AIAA Paper 87-0109, Jan. 1987.

[6]Batina, J. T., Seidel, D. A., Bland, S. R., and Bennett, R. M., "Unsteady Transonic Flow Calculations for Realistic Aircraft Configurations," AIAA Paper 87-0850, April 1987.

[7]Bennett, R. M., Bland, S. R., Batina, J. T., Gibbons, M. D., and Mabey, D. G., "Calculation of Steady and Unsteady Pressures on Wings at Supersonic Speeds with a Transonic Small-Disturbance Code," AIAA Paper 87-0851, April 1987.

[8]Yates, E. C., Jr., Land, N. S., and Foughner, J. T., Jr., "Measured and Calculated Subsonic and Transonic Flutter Characteristics of a 45-Deg Sweptback Wing Planform in Air and in Freon-12 in the Langley Transonic Dynamics Tunnel," NASA TN D-1616, March 1963.

[9]Yates, E. C., Jr., "AGARD Standard Aeroelastic Configurations for Dynamic Response. Candidate Configuration 1:—Wing 445.6," NASA TM 100492, Aug. 1987.

[10]Sandford, M. C., Abel, I., and Gray, D. L., "Development and Demonstration of a Flutter-Suppression System Using Active Controls," NASA TR R-450, Dec. 1975.

[11]Sandford, M. C., Ruhlin, C. L., and Abel, I., "Transonic Flutter Study of a 50.5-Deg Cropped-Delta Wing with Two Rearward-Mounted Nacelles," NASA TN D-7544, 1974.

[12]Cunningham, H. J., Batina, J. T., and Bennett, R. M., "Modern Wing-Flutter Analysis by Computational Fluid Dynamics Methods," American Society of Mechanical Engineers, Paper 87-WA/Aero-9, Dec. 1987.

[13]Batina, J. T., "Unsteady Transonic Algorithm Improvements for Realistic Aircraft Applications," AIAA Paper 88-0105, Jan. 1988.

[14]Batina, J. T., "Unsteady Transonic Small-Disturbance Theory Including Entropy and Vorticity Effects," AIAA Paper 88-2278, April 1988.

[15]Edwards, J. W., Bennett, R. M., Whitlow, W., Jr., and Seidel, D. A., "Time-Marching Transonic Flutter Solutions Including Angle-of-Attack Effects," *Journal of Aircraft,* Vol. 20, Nov. 1983, pp. 899–906.

[16]Edwards, J. W., Bennett, R. M., Whitlow, W., Jr., and Seidel, D. A., "Time-Marching Transonic Flutter Solutions Including Angle-of-Attack Effects," AIAA Paper 82-3685, May 1982.

[17]Bennett, R. M. and Desmarais, R. N., "Curve Fitting of Aeroelastic Transient Response Data with Exponential Functions," *Flutter Testing Techniques,* NASA SP-415, May 1975, pp. 43–58.

[18]Desmarais, R. N. and Bennett, R. M., "User's Guide for a Modular Flutter Analysis Software System (FAST Version 1.0)," NASA TM 78720, May 1978.